

Elastic, Inelastic, and Path Length Fluctuations in Jet Tomography

Simon Wicks,¹ William Horowitz,¹ Margdalena Djordjevic,^{1,2} and Miklos Gyulassy¹¹Department of Physics, Columbia University, 538 West 120-th Street, New York, NY 10027²Department of Physics, The Ohio State University,

191 West Woodruff Avenue, Columbus, OH 43210

(Dated: November 1, 2018)

We propose a possible perturbative QCD solution to the heavy quark tomography problem posed by recent non-photonic single electron data from central Au+Au collisions at $\sqrt{s} = 200$ GeV. Jet quenching theory is extended to include (1) elastic as well as (2) inelastic parton energy losses and (3) jet path length fluctuations. The three effects combine to reduce the discrepancy between theory and the data without violating the global entropy bounds from multiplicity and elliptic flow data. We also check for consistency with the pion suppression data out to 20 GeV. Fluctuations of the geometric jet path lengths and the difference between the widths of fluctuations of elastic and inelastic energy loss play essential roles in the proposed solution.

PACS numbers: 12.38.Mh; 24.85.+p; 25.75.-q

Light quark and gluon jet quenching observed via suppression [1] in Cu+Cu and Au+Au collisions at $\sqrt{s} = 62 - 200$ GeV at the Relativistic Heavy Ion Collider (RHIC) has been remarkably consistent thus far with predictions [2]-[5]. However, recent non-photonic single electron data [6, 7] (which present an indirect probe of heavy quark energy loss) have significantly challenged the underlying assumptions of the jet tomography theory (see [8]). A much larger suppression of electrons than predicted was observed in the $p_T > 4 - 8$ GeV region (see Fig. 1). These data falsify the assumption that heavy quark quenching is dominated by radiative energy loss when the bulk QCD matter parton density is constrained by the observed $dN/dy = 1000$ rapidity density of produced hadrons.

The observed "perfect unity" [10, 11] of the sQGP at long wavelengths ($p_T < 2$ GeV/c) provides direct evidence for highly nonperturbative bulk dynamics [9, 12]. However, due to asymptotic freedom, a breakdown of perfect unity and nonperturbative effects is expected at p_T several times greater than the mean thermal energy, $3T = 1 - 2$ GeV. Prior to these electron data, pQCD based jet quenching theory provided in fact increasingly reliable predictions above $p_T > 5 - 7$ GeV [10, 13] for the nuclear modification of light parton jets [2]-[5]. The non-photonic electron data raise the question of whether the novel nonperturbative physics of the strongly interacting Quark Gluon Plasma (sQGP) [9] produced at RHIC could persist down to much smaller wavelengths, $1=p_T = 1=50$ fm/c, than previously expected. This question is also of pragmatic importance because high p_T jets can be utilized as effective "external" tomographic probes of the bulk sQGP matter only if their dynamics can be predicted reliably. Otherwise, jet quenching is merely an additional signal of new physics instead of a calibrated diagnostic probe of that physics.

The upper band of Fig. 1 shows that the predictions from [8] considerably underestimated the electron nuclear modification even out to $p_T = 8$ GeV. This discrepancy points to either (1) missing perturba-

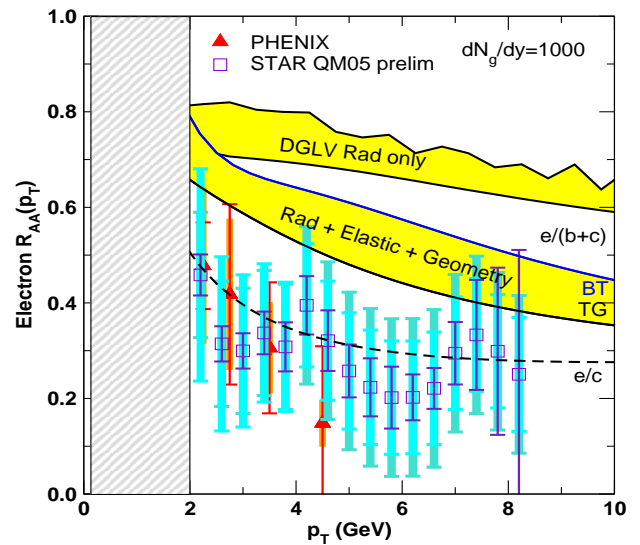


FIG. 1: The suppression factor, $R_{AA}(p_T)$, of non-photonic electrons from decay of quenched heavy quark ($c+b$) jets is compared to PHENIX [6] and preliminary STAR data [7] data in central Au+Au reactions at 200 GeV. Shaded bars indicate systematic errors, while thin error lines indicate statistical ones. All calculations assume initial $dN_g/dy = 1000$. The upper yellow band from [8] takes into account radiative energy loss only, using a fixed $L = 6$ fm; the lower yellow band is our new prediction, including both elastic and inelastic energy losses as well as jet path length fluctuations. The bands provide an estimate of current theoretical uncertainties. The dashed curve shows the electron suppression using inelastic and TG elastic energy loss with bottom quark jets neglected.

tive QCD physics, (2) incomplete understanding of the initial heavy quark production and/or (3) novel non-perturbative mechanisms affecting partonic physics out to $p_T > 10$ GeV. We note that $p_T > 8$ GeV (single non-photonic) electrons originate in our calculations from the fragmentation and decay of both charm and bottom quarks with transverse momenta $p_T > 12 - 4$ GeV (see

Fig. 5 in [8]).

Possibility (3) is of course the most radical and would imply the persistence of non-perturbative physics in the sQGP down to extremely short wavelengths, i.e. $1=p_T = 1=50\text{fm}$. Processes can be postulated to improve the fit to the data [14], but at the price of losing theoretical control of the tomographic information from jet quenching data. DGVW [8] showed that by arbitrarily increasing the initial sQGP densities to unphysical $dN_g=dy > 4000$, the non-photonic electrons from heavy quarks can be artificially suppressed to $R_{AA} < 0.5 - 0.1$. Thus conventional radiative energy loss requires either violation of bulk entropy bounds or nonperturbatively large extrapolations of the theory. Even when ignoring the bottom contribution, Ref. [15], found that a similarly excessive transport coefficient [16], $\Phi_{\text{eff}} = 14 \text{ GeV}^2/\text{fm}$, was necessary to approach the measured suppression of electrons from charm jet decay.

The main theoretical problem is that bottom quark jets are too weakly quenched by radiative energy loss. Their contribution significantly reduces the single electron suppression [8] compared to that of the charm jets alone. While the current data cannot rule out the possibility (2) that the bottom production in this kinematic range is overestimated in NLO theory [17, 18], in this paper we pursue the more conservative approach of examining the inclusion of a previously neglected pQCD component of the physics.

The recent papers [19, 20] motivated us to revisit the assumption that pQCD elastic energy loss [21] is negligible compared to radiative. In earlier studies, the elastic energy loss [21, 22, 23, 24, 25, 26] was found to be $dE_{\text{el}}=dx = 0.3 - 0.5 \text{ GeV/fm}$, which was erroneously considered to be small compared to the several GeV/fm expected from radiative energy loss. The apparent weakness of conventional pQCD collisional energy loss mechanisms was also supported by parton transport theory results [27]–[28], which showed that the typical thermal pQCD elastic cross section, $\text{el} = 3\text{mb}$, is too small to explain the differential elliptic flow at high $p_T > 2 \text{ GeV}$ and also underestimates the high p_T quenching of pions.

In contrast, Mustafa [19] found that radiative and elastic energy losses for heavy quarks were in fact comparable over a very wide kinematic range accessible at RHIC. In Fig. 2, we confirm Mustafa's finding and extend it to the light quark sector as well. The fractional energy loss, $E = E_{\text{el}}/E$, from DGLV radiative for $u; c; b$ quarks (solid curves; see also App. IB) is compared to TG [22] and BT [23] estimates of elastic (dashed curves; see also App. IA). For light quarks, the elastic energy loss decreases more rapidly with energy than radiative energy loss, but even at 20 GeV the elastic is only 50% smaller than the radiative.

From Fig. 2, we see that above $E > 10 \text{ GeV}$, the light and charm quarks have similar elastic and inelastic energy losses. But due to the large mass effect [29]–[34], [15], both radiative and elastic energy losses remain significantly smaller for bottom quarks than for light and

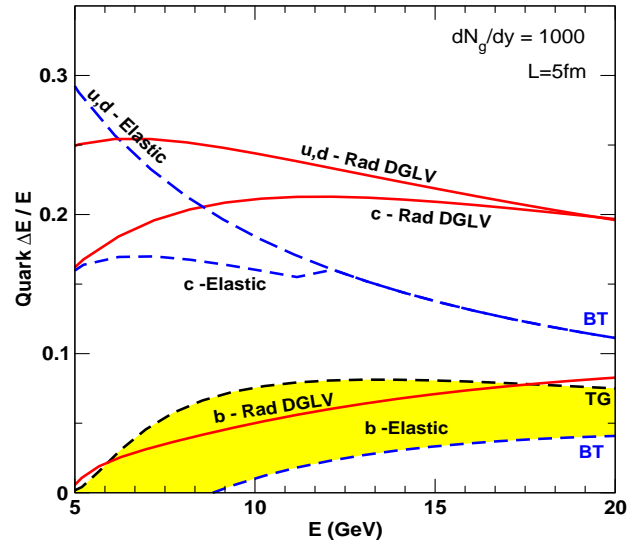


FIG. 2: $E = E_{\text{el}}/E$ for $u; c; b$ quarks as a function of E . A Bjorken expanding QGP with path length $L = 5 \text{ fm}$ and initial density fixed by $dN_g=dy = 1000$ is assumed. The curves are computed with the coupling $\alpha_s = 0.3$ held fixed. For DGLV mass $m_D = (dN_g=dy)^{1/3}$, the gluon mass is $m_D = 2$, the light quark mass is $m_D = 2$, the charm mass is 1.2 GeV , and the bottom mass is 4.75 GeV . Radiative DGLV first order energy loss is compared to elastic parton energy loss (in TG or BT approximations). The yellow bands provide an indication of theoretical uncertainties in the elastic energy loss for bottom quarks.

charm quarks. We present both TG and BT as a measure of the theoretical uncertainties of the Coulomb log (see App IC for benchmark numerical examples). These are largest for the heaviest b quark, for which the leading log approximation [22, 23] breaks down in the kinematic range accessible at RHIC as they are not ultrarelativistic. More rigorous computations of elastic energy loss [45] or advanced numerical covariant transport techniques [27] can be used to reduce considerably the theoretical uncertainties on the elastic energy loss effects.

Theoretical Framework

The quenched spectra of partons, hadrons, and leptons are calculated as in [8] from the generic pQCD convolution

$$\frac{E d^3 \langle e \rangle}{dp^3} = \frac{E_i d^3 \langle Q \rangle}{dp_i^3} P(E_i \rightarrow E_f) D(Q \rightarrow H_Q) f(H_Q \rightarrow e); \quad (1)$$

where Q denotes quarks and gluons. For charm and bottom, the initial quark spectrum, $E d^3 \langle Q \rangle = dp^3$, is computed at next-to-leading order using the code from [17, 18]; for gluons and light quarks, the initial distributions are computed at leading order as in [5]. $P(E_i \rightarrow E_f)$ is the energy loss probability, $D(Q \rightarrow H_Q)$ is the fragmentation function of quark Q to hadron H_Q , and $f(H_Q \rightarrow e)$ is the decay function of hadron H_Q into the observed single electron. We use the same mass and factorization

scales as in [35] and employ the CTEQ 5M parton densities [36] with no intrinsic k_T . As in [35] we neglect shadowing of the nuclear parton distribution in this application.

We assume that the final quenched energy, E_f , is large enough that the Eikonal approximation can be employed. We also assume that in Au+Au collisions, the jet fragmentation function into hadrons is the same as in e^+e^- collisions. This is expected to be valid in the deconfined PQCD medium case, where hadronization of $Q \bar{Q}$ cannot occur until the quark emerges from the deconfined SQGP medium.

The main difference between our previous calculation [8] and the present one is the inclusion of two new physics components in the energy loss probability $P(E_i \rightarrow E_f)$. First, $P(E_i \rightarrow E_f)$ is generalized to include for the first time both elastic and inelastic energy loss and their fluctuations. We note that Vitev [37] was the first to generalize GLV to include initial state elastic energy loss effects in D+Au. In this work, Eq. (2) extends the formalism to include final state elastic energy loss effects in A+A.

The second major change relative to our previous applications is that we now take into account geometric path length fluctuations as follows:

$$P(E_i \rightarrow E_f) = \frac{d}{2} \int \frac{d^2 \mathbf{x}_i}{N_{\text{bin}}(b)} T_{AA}(\mathbf{x}_i; \mathbf{b}) P_{\text{rad}}(E_i \rightarrow E_f; L(\mathbf{x}_i; \mathbf{b})) P_{\text{el}}(E_i \rightarrow E_f; L(\mathbf{x}_i; \mathbf{b})). \quad (2)$$

Here

$$L(\mathbf{x}_i; \mathbf{b}) = \int d\mathbf{p}_i(\mathbf{x}_i + \hat{\mathbf{n}}(\mathbf{b})) = h_{\mathbf{p}_i} \quad (3)$$

is the locally determined effective path length of the jet given its initial production point \mathbf{x}_i and its initial azimuthal direction relative to the impact parameter plane $(\mathbf{x}; \mathbf{y})$. The geometric path averaging used here is similar to that used in [38] and by Eskola et al. [39]. However, the inclusion of elastic energy losses together with path fluctuations in more realistic geometries was not considered before.

We consider a diffuse Woods-Saxon nuclear density profile [40], which creates a participant transverse density, $\rho(\mathbf{x}_i)$, computed using the Glauber profiles, $T_A(\mathbf{x})$, with inelastic cross section $\sigma_{NN} = 42 \text{ mb}$. The bulk SQGP transverse density is assumed to be proportional to this participant density, and its form is shown (for the $\mathbf{y} = 0$ slice) in Fig. 4 by the curve labeled $_{QGP}$. The distribution of initial hard jet production points, \mathbf{x}_i , is assumed on the other hand to be proportional to the binary collision density, $T_{AA} = T_A(\mathbf{x} + \mathbf{b} = 2)T_A(\mathbf{x} - \mathbf{b} = 2)$. This is illustrated in Fig. 4 by the narrower curve labeled $_{\text{jet}}$.

The combination of fluctuating DGLV radiative [30] with the new elastic energy losses and fluctuating path lengths (via the extra $d^2 \mathbf{x}_i$, d integrations) adds a high

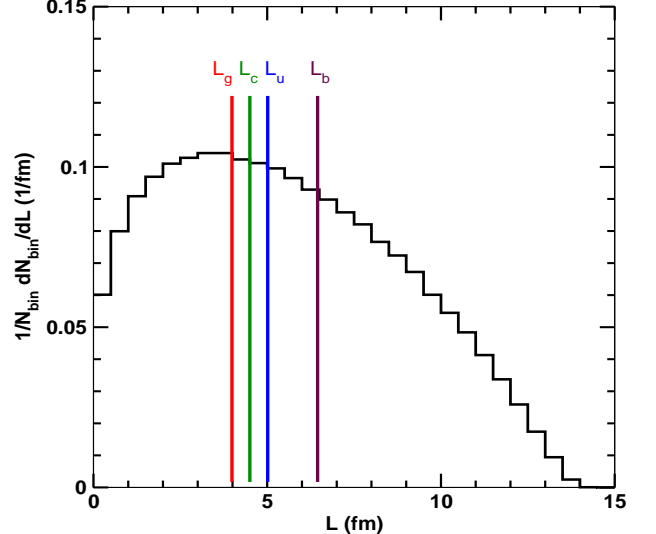


FIG. 3: Distribution of path lengths (given by Eq. (3)) traversed by hard scatterers in 0-5% most central collisions; the lengths, $L(\mathbf{x}_i; \mathbf{b})$, are weighted by the probability of production and averaged over azimuth. An equivalent formulation of Eq. (4) is $R_Q^I = \int dL \int N_{\text{bin}} dN_{\text{bin}} = dL \int (1 - \bar{\rho}) P_Q^I(\mathbf{x}; L)$. Since $\int N_{\text{bin}} dN_{\text{bin}} = dL$ is a purely geometric quantity, it is the same for all jet varieties. Also displayed are the single, representative path lengths, L_Q , used as input in approach II. Note the hierarchy of scales with glue requiring the shortest, then charm, light quarks, and bottom the longest effective path length.

computational cost to the extended theory specified by Eqs. (1,2). In this first study with the extended theory, we explore the relative order of magnitude of the competing effects by combining two simpler approaches.

In approach I, we parameterize the heavy quark PQCD spectra by a simpler power law, $E d^3 Q = d^3 k / 1 - p_T^{n+2}$, with a slowly varying logarithmic index $n = n(p_T)$. For the pure power law case, the partonic modification factor, $R_Q = d_Q^{\text{final}} / d_Q^{\text{initial}}$, (prior to fragmentation) is greatly simplified. This enables us to perform the path length fluctuations numerically via

$$R_Q^I = \frac{d}{2} \int \frac{d^2 \mathbf{x}_i}{N_{\text{bin}}(b)} T_{AA}(\mathbf{x}_i; \mathbf{b}) \int (1 - \bar{\rho}) P_Q^I(\mathbf{x}; L(\mathbf{x}_i; \mathbf{b})), \quad (4)$$

where

$$P_Q^I(\mathbf{x}; L) = \int d\mathbf{p}_i P_{Q,\text{rad}}(\mathbf{x}; L) P_{Q,\text{el}}(\mathbf{x}; L); \quad (5)$$

Both the mean and width of those fractional energy losses depend on the local path length. (See App D for numerical illustrations of Eq.(5) for a fixed $L = 5 \text{ fm}$ light quark case.)

We emphasize, however, that no externally specified a priori path length, L , appears in Eq. (4); the path lengths are allowed to explore the whole geometry. Fig. 3 shows

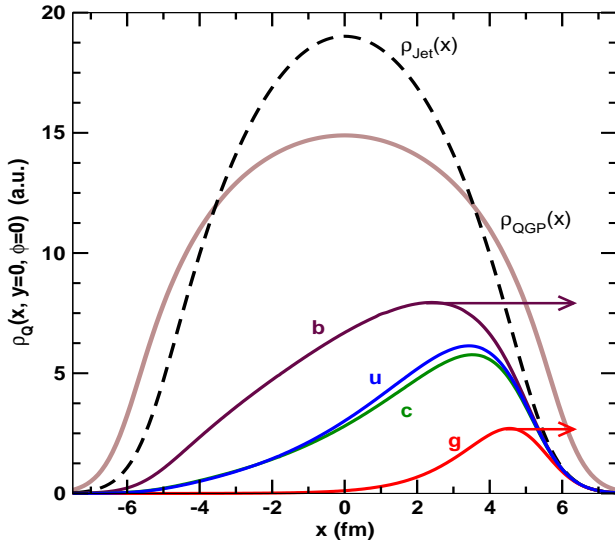


FIG. 4: Transverse coordinate ($x; 0$) distribution of surviving $p_T = 15$ GeV, $Q = g; u; c; b$ jets moving in direction $\phi = 0$ as indicated by the arrows. Units are arbitrary for illustration. The transverse (binary collision) distribution of initial jet production points, $\rho_{\text{jet}}(x; 0)$, is shown at midrapidity for $A + A$ collisions at $b = 2.1$ fm. The ratio $\rho = \rho_{\text{jet}}$ (see Eq.(8)) gives the local quenching factor including elastic and inelastic energy loss through the bulk QGP matter distributed as $\rho_{\text{QGP}}(x; 0)$.

the broad distribution of lengths probed by hard partons in approach I.

In the second approach, we determine effective path lengths, L_Q , for each parton flavor, Q , by varying fixed L predictions $R_Q^{\text{II}}(p_T; L)$ and comparing to approach I; see Fig. 3. In approach II, $R_Q^{\text{II}}(p_T; L)$ is calculated directly from Eq. (1) with $P(E_i \mid E_f)$ in Eq. (2) replaced by the fixed L approximation

$$P(E_i \mid E_f; L) = P_{\text{rad}}(E_i \mid E_f; L) + P_{\text{el}}(E_i \mid E_f; L); \quad (6)$$

Here, jet quenching is performed via two independent branching processes in contrast to the additive convolution in Eq. (4). For small energy losses the two approaches are similar. They differ however in the case of long path lengths when the probability of complete stopping approaches unity. In the convolution method, the probability of $\eta > 1$ is interpreted as complete stopping, whereas in the branching algorithm the long path length case is just highly suppressed. In both cases we take into account the small finite probability that the fractional energy loss $\eta \rightarrow 0$ due to fluctuations.

To illustrate the difference in approach II, consider the case of power law initial Q distributions as in Eq. (4). In this case

$$R_Q^{\text{II}}(p_T; L_Q) = h(1 - \frac{p_T}{L_Q})^n (1 - \frac{p_T}{L_Q})^n \quad (7)$$

The branching implementation is seen via the product of two distinct factors in contrast to the one quenching factor in Eq. (4). For small η both approaches obviously give rise to the same $R_Q = 1 - nh_Q$.

In both approaches, fluctuations of the radiative energy loss due to gluon number fluctuations are computed as discussed in detail in Ref. [8, 33]. This involves using the DGLV generalization [30] of the GLV opacity expansion [3] to heavy quarks. Bjorken longitudinal expansion is taken into account by evaluating the bulk density at an average time $t = L/2$ [8, 33]. For elastic energy loss fluctuations, the full Fokker-Planck solution applicable for small fractional energy loss is approximated by a Gaussian centered at the average energy loss with variance $\sigma_{\text{el}}^2 = 2T h E^{\text{el}}(p_T; L)$ [28]. In approach I the correct, numerically intensive integration through the Bjorken expanding medium provides $E^{\text{el}}(p_T; L)$. In approach II the $L = 2$ approximation is again used; numerical comparisons show that for $L = 2 - 7$ fm this reproduces the full calculation well. Finally, we note that we use the additional numerical simplification of keeping the strong coupling constant α_s fixed at 0.3.

Numerical Results: Parton Level

In Fig. 5, we show the quenching pattern of Q from the second approach for a "typical" path length scale $L = 5$ fm, similar to that used in previous calculations [8]. The curves show $R_Q(p_T)$, prior to hadronization, for $Q = g; u; c; b$. The dashed curves show the quenching arising from only the DGLV radiative energy loss. The solid curves show the full results after including TG elastic as well as DGLV radiative energy loss. Adding elastic energy loss is seen to increase the quenching of all flavors for fixed path length. Note especially the strong non-linear increase of the gluon suppression and the factor 2 increase of the bottom suppression. The curious switch of the u and the c quenching reflects the extra valence (smaller index n_u) contribution to light quarks.

Fig. 5 emphasizes the unavoidable result of using a fixed, "typical" path length scale, L , in jet tomography: the pion and single electron quenching can never be similar. If pions were composed only of light quarks and electrons only of charm, then we would expect comparable quenching for both. However, contributions from highly quenched gluons decrease the pion R_{AA} while weakly quenched bottom quarks increase the electron R_{AA} . Therefore, in the fixed length scenario, we expect a noticeable difference between pion and single electron suppression patterns.

In Fig. 4 we use fluctuating path lengths. The solid curves labeled by the parton flavor $Q = g; u; c; b$ show the relative transverse coordinate density of surviving jets defined by

$$\rho_Q(x; \eta) = \rho_{\text{jet}}(x) \cdot d(\eta) \cdot P_Q^{\text{II}}(\eta; L(x; \eta)); \quad (8)$$

ρ_Q is given by the initial transverse x production distribution times the quenching factor from that position in direction with transverse momentum p_T . The case shown is

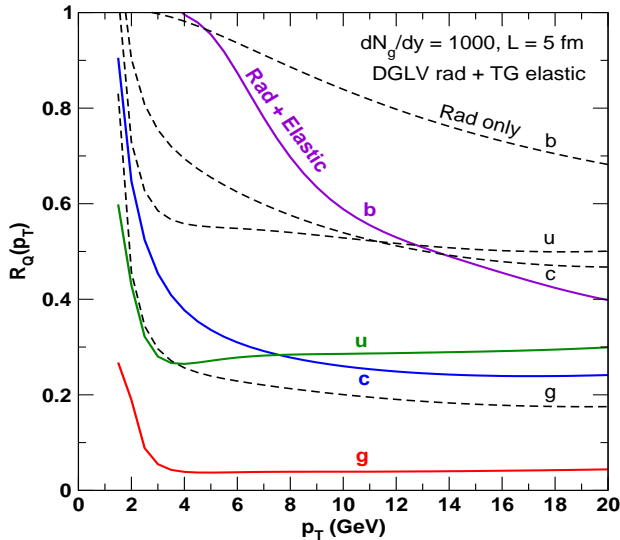


FIG. 5: Partonic nuclear modification, $R_Q^{II}(p_T)$ via Eq.(7), for $g;u;c;b$ as a function of p_T for xed $L = 5$ fm path length and $dN_g/dy = 1000$. Dashed curves include only radiative energy loss, while solid curves include elastic energy loss as well.

for a $p_T = 15$ GeV jet produced initially at $(x; 0)$ and moving in the direction $\hat{n} = 0$ along the positive x axis. The quenching is determined by the participant bulk matter along its path $_{QGP}(x + vt; 0; t)$, and varies with x because the local path length $L = L(x; 0; 0)$ changes according to Eq. (3).

What is most striking in Fig. 4 is the hierarchy of Q -dependent length scales. No single, representative path length can account for the distribution of all flavors. In general heavier flavors are less biased toward the surface (in direction \hat{n}) than lighter flavors since the energy loss decreases with the parton mass. Gluons are more surface biased than light quarks due to their color Casimir enhanced energy loss. In addition, note the surprising reversal of the u and c suppressions, also seen in Fig. 5. Fig. 2 shows that the energy loss of c is somewhat less than for u ; however, the higher p_T power index, n , of c relative to u (as predicted by pQCD and due to the valence component of u) compensates by amplifying its quenching.

However, it is clear that none of the distributions can be usefully categorized as surface emission. The characteristic widths of these distributions range from $x = 3 - 6$ fm. Such a large dynamical range of path length fluctuations allows for the consistency of simultaneously reproducing both the electron and pion data.

We turn next to Figs. 6 and 7 to show the interplay between dynamical geometry seen in Fig. 4 and the elastic-enhanced quenching of partons. In Figs. 6 and 7 the solid green curves labeled "DGLV+TG/BT : Full Geometry" are the results using approach I based on Eq. (4). The curves labeled TG and BT are from approach II based on Eq. (7). The effective xed L_Q in II were taken to match approximately the green curves in which full path length

fluctuations are taken into account. This procedure is not exact because of the different numerical approximations involved, but the trends are well reproduced. The L_Q are determined only to 0.5 fm accuracy, as this suffices for our purposes here. We show the comparison between approaches I and II for heavy quarks in Fig. 6 using $L_c = 4.5$ and $L_b = 6.5$ fm and for gluons and light quarks in Fig. 7 using $L_g = 4.0$ and $L_u = 5.0$ fm; see Fig. 3 for a visual comparison of the input length distributions used. This hierarchy of Q -dependent length scales is in accord with that expected from Fig. 4.

Note that in comparison to the xed $L = 5$ fm case in Fig. 5, geometric fluctuations reduce gluon jet quenching in Fig. 7 by a factor 2 relative to the xed L . Nevertheless, even with path length fluctuations the gluons are still quenched by a factor of 10 when elastic energy loss is included in addition to radiative.

The amplified role of elastic energy loss is due to its smaller width for fluctuations relative to radiative fluctuations. Even in moderately opaque media with $L = 10$, inelastic energy loss fluctuations are large because only a few, 2-3, extra gluons are radiated [4]. Thus, gluon number fluctuations, $O(1/N_g)$ lead to substantial reduction in the effect of radiative energy loss. On the other hand, elastic energy loss fluctuations are controlled by collision number fluctuations, $O(1/L)$, which are small in comparison. Therefore, fluctuations of the elastic energy loss do not dilute the suppression of the nuclear modification.

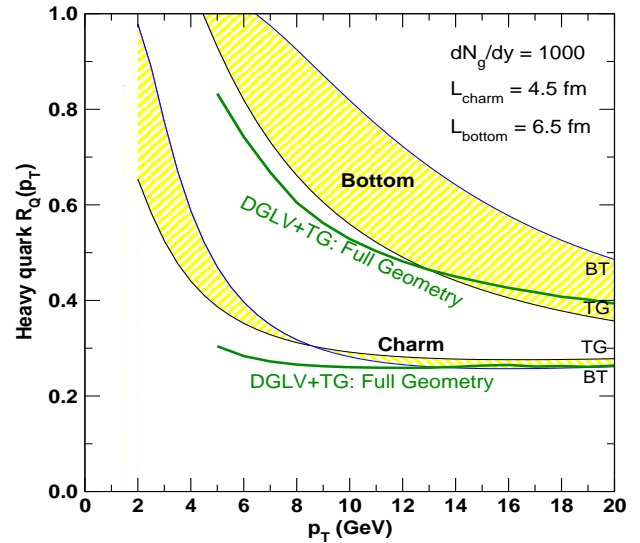


FIG. 6: Heavy quark jet quenching before fragmentation into mesons for $dN_g/dy = 1000$. Solid green curves show the results of approach I based on Eq. (4) including full geometric path length fluctuations and DGLV radiative and TG elastic energy loss for c and b quarks. Upper and lower yellow bands show predictions using approach II via Eq. (7) with effective path lengths taken as $L_c = 4.5$ and $L_b = 6.5$ fm. As previously noted in Fig. 2, the difference between TG and BT curves indicates the magnitude of theoretical uncertainties in the elastic energy loss.

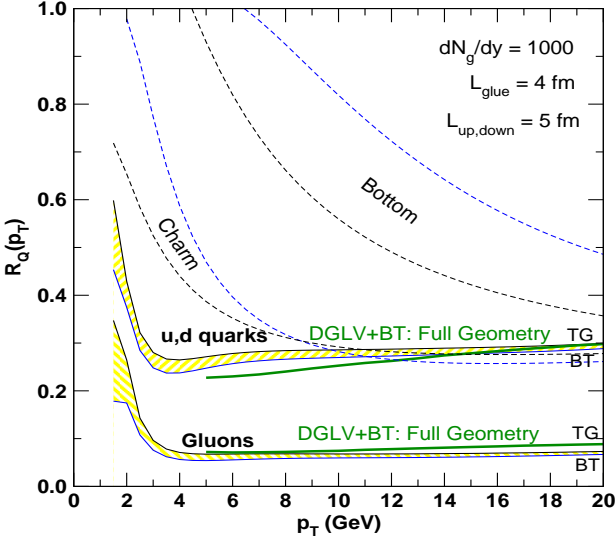


FIG . 7: As in Fig. 6 but for light $u; d$ quarks and gluons. The yellow bands are computed in this case with the effective gluon path lengths $L_g = 4.0$ and $L_u = 5.0$ fm based on Eq. (7). Note that charm and light quark quenching are similar in this p_T range.

tion factor as much as N_g fluctuations. The increase in the sensitivity of the final quenching level to the opacity is a novel and useful byproduct of including the elastic channel; see Fig. 11 in Appendix D. The inclusion of elastic energy loss significantly reduces the fragility of pure radiative quenching [39] and therefore increases the sensitivity of jet quenching to the opacity of the bulk medium [41].

Numerical Results: Pions and Electrons

We now return to Fig. 1 to discuss the consequence of including elastic energy loss of c and b on the electron spectrum. The largest source of uncertainty, represented by the lower yellow band, is the modest but poorly determined elastic energy loss, $E = E_{\text{inel}} = 0.0 - 0.1$, of bottom quarks (see Fig. 2). Nevertheless, it is remarkable that the lower yellow band can reach $R_{AA}^e = 0.5$ in spite of keeping $dN_g/dy = 1000$, consistent with measured multiplicity, and using a conservative $s = 0.3$. While the preliminary data suggest that $R_{AA}^e < 0.4$, the R_{AA}^e band is not inconsistent with the preliminary data above $p_T > 7$ GeV within present experimental and theoretical errors. Our tentative conclusion, therefore, is that the combined elastic and inelastic pQCD approach may solve a substantial part of the heavy quark quenching puzzle.

However, as emphasized in [8], any proposed solution of this puzzle must also be checked for consistency with the extensive pion quenching data [1], for which preliminary data now extend out to $p_T = 20$ GeV. That this is a challenge is clearly seen in Fig. 5, where for fixed $L = 5$ fm, the addition of elastic energy loss would overpredict the quenching of pions. However, the simultaneous inclusion of path fluctuations leads to a decrease of the mean $u; d$ path lengths that partially offsets the increased energy loss. Therefore, the combined three effects con-

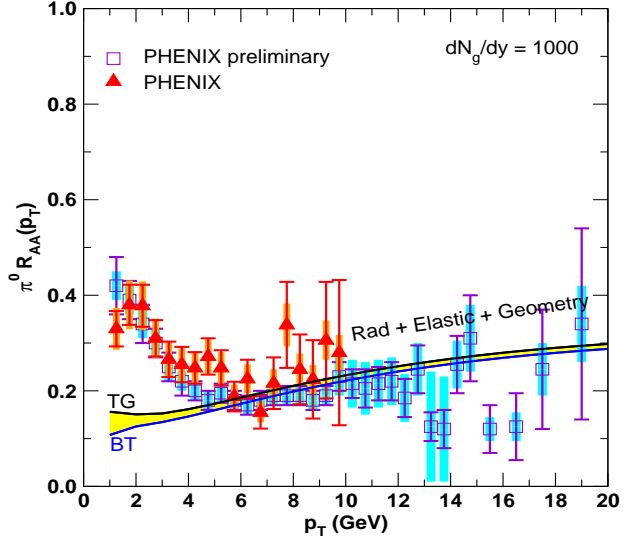


FIG . 8: The consistency of the extended jet quenching theory is tested by comparing its prediction to the nuclear modification of the π^0 spectra observed by PHENIX [1].

sidered here makes it possible to satisfy $R_{AA}^e < 0.5$ without violating the bulk $dN_g/dy = 1000$ entropy constraint and without violating the pion quenching constraint $R_{AA}^e = 0.2 - 0.1$ now observed out to 20 GeV; see Fig. 8. We note that the slow rise of R_{AA}^e with p_T in the present calculation is due in part to the neglect of initial k_T smearing that raises the low p_T region and the EMC effect that lowers the high p_T region (see [5]).

Conclusions

While the results presented in this paper are encouraging, further improvements of the jet quenching theory will be required before stronger conclusions can be drawn. More work is needed to sort out coherence and correlation effects between elastic and inelastic processes that occur in a finite time and with multiple collisions. Classical electrodynamics calculations presented in [42] suggested that radiative and elastic processes could destructively interfere over lengths far longer than previously thought. However, the formalism used does not disentangle known radiative Ter-Mikaelian effects [43] from expected finite size collisional effects, and does not include transition radiation [47]. More importantly, the authors inconsistently treat their current as conserved (using $j^0 = k_j \cdot \mathbf{v} = 0$) while simultaneously dropping the backwards-moving partner parton term from the current (thus violating current conservation by producing, at a finite time, a charge without a corresponding opposite charge); this results in a spurious subtraction of the (negative) binding energy of the pair and a correspondingly drastic reduction in the elastic energy loss. As described in [44], a proper accounting of the current shows finite size effects persist out only to the expected lengths of order the screening scale, $1 = \alpha_D^{-1} \approx 1$ fm. Recent work on the quantum mechanical treatment of elastic energy loss in a finite medium [45, 46] also con-

cluded that finite size effects on R_{AA} remain small except in peripheral collisions.

There are several other open problems that require further study. The radiative and elastic energy losses depend sensitively on the coupling, $E^{\text{rad}} / \frac{3}{s}$ and $E^{\text{el}} / \frac{2}{s}$. Future calculations will have to relax the current fixed s approximation and allow it to run. The energy loss involves integrals that probe momentum scales that are certainly nonperturbative. Therefore it will be important to study the irreducible uncertainty associated with the different maximum s cuts prescriptions commonly used. Further, improved numerical techniques will have to be devised to overcome the limitations of the approximate, two-step approach employed here to incorporate the essential path length fluctuations. From an experimental perspective, direct measurement of D spectra would be most valuable to separate the di erent bottom and charm jet quark dynamics that are at present convoluted in the electron spectra.

Acknowledgments: Valuable input from Azfar Adil on parton spectra and discussions with Xiang Dong, Barbara Jacak, John Harris, Peter Levai, Denes Molnar, Thomas Ulrich, Ivan Vitev, Xian-Nian Wang, and Nu Xu are gratefully acknowledged. This work is supported by the Director, Office of Science, Office of High Energy and Nuclear Physics, Division of Nuclear Physics, of the U.S. Department of Energy under Grants No. DE-FG02-93ER40764. M.D. acknowledges support by the U.S. Department of Energy under Grants No. DE-FG02-01ER41190 during the final parts of this work.

I. APPENDIX

A. Collisional Energy Loss

The leading logarithmic expression for the elastic energy loss of a jet with color C and C_R in an ideal quark-gluon plasma with n_f active quark flavors and temperature, T , is given by [21]

$$\frac{dE^{\text{el}}}{dx} = C_R \frac{2}{s} T^2 \left(1 + \frac{n_f}{6}\right) f(v) \log(B_c) \quad (9)$$

where the Coulomb log is controlled by the ratio B_c that involves relevant minimum and maximum momentum transfers or impact parameters. For scattering in an assumed ultrarelativistic ($m = 0$) gas of partons the jet velocity dependence is

$$f(v) = \frac{1}{v^2} \left(v + \frac{1}{2}(v^2 - 1)\right) \log\left(\frac{1+v}{1-v}\right)^{v!} \frac{1}{1} \quad (10)$$

Estimates for B_c differ below asymptotic ($E = T$) energies and are given in [21], [22], and [23] that we denote by B_{TG} and B_T respectively:

$$B_{Bj} = (4E_p T)^2$$

$$\begin{aligned} B_{TG} &= \frac{4pT}{(E_p + p + 4T)} = () \\ &\approx \frac{n_f}{2^{6+n_f}} 0.85 E_p T = \frac{2}{3} E_p \frac{M^2}{T} \\ B_B &= \frac{n_f}{4^{6+n_f}} 0.36 \frac{(E_p T)^2}{M^2} = \frac{2}{3} E_p \frac{M^2}{T} \end{aligned} \quad (11)$$

with the crossover between $E_p \frac{M^2}{T}$ and $E_p \frac{M^2}{T}$ being taken at $E_p = \frac{2M^2}{T}$ for numerical computation.

B. DGLV Radiative Energy Loss

For completeness we also record the DGLV formula for radiative energy loss used in our calculations. We neglect finite kinematic limits on the momentum transfer q integral, and perform the finite $0 < k_T < k_{\text{max}} = 2px(1-x)$ and azimuthal $0 < \phi < \pi$ integrations analytically. The mean fractional radiative energy loss can be then evaluated numerically from the expression

$$\frac{E_{\text{ind}}^{(1)}}{E} = \frac{C_F}{g} \frac{s}{L} \int_0^{\frac{m_g}{E_p + p}} dx \frac{Z_1 \frac{M}{E_p + p}}{Z_1} \frac{4^2 q^3 dq}{\left(\frac{4E_x}{L}^2 + (q^2 + \frac{2}{2})^2\right)} (A \log B + C) \quad (12)$$

where

$$Z^2 = m_g^2 (1-x) + M^2 x^2 \quad (13)$$

$$Z^1 = g_{gg} + q_{gg} \quad (14)$$

$$g_{gg} = \frac{9}{2} \frac{s}{2} \text{ and } q_{gg} = \frac{4}{9} g_{gg} : \quad (15)$$

We employ the asymptotic 1-loop transverse gluon mass $m_g = \sqrt{\frac{2}{3}}$. The A, B, C functions denote

$$A = \frac{2}{f^3} \frac{2}{f^2} + q^2 \quad (16)$$

$$B = \frac{(\frac{2}{2} + K)(\frac{2}{2} Q - K)}{\frac{2}{2} (\frac{2}{2} Q - K) Q K + Q^+ Q^+ + f f} \quad (17)$$

$$\begin{aligned} C &= \frac{1}{2q^2 f^2 f} \frac{2}{2} \frac{2}{2} (2q^2 - 2) + \frac{2}{2} \frac{2}{2} (2q^2 - 2) K \\ &+ Q^+ (\frac{4}{2} - 2\frac{2}{2} Q^+) + f (\frac{2}{2} (\frac{2}{2} - 3\frac{2}{2} + \frac{2}{2}) \\ &+ 2q^2 Q^+) + 3 \frac{2}{2} q^2 Q_k \end{aligned} \quad (18)$$

where the abbreviated symbols denote

$$K = k_{\text{max}}^2 = 2px(1-x) \quad (19)$$

$$Q = q^2 \quad (20)$$

$$Q_k = q^2 K^2 \quad (21)$$

$$f = f(\frac{2}{2} Q, \frac{2}{2} Q^+) \quad (22)$$

$$f = f(\frac{2}{2} Q^+, \frac{2}{2} Q_k) \quad (23)$$

$$\text{with } f(x, y, z) = \frac{p}{x^4 + 2x^2 y + z^2}.$$

E_{jet} (GeV)	Radiative $\frac{E}{E}$		Collisional $\frac{E}{E}$		
	DGLV	Bj	TG	BT	
10	0.2111	0.2022	0.1594	0.1596	
11	0.2126	0.1894	0.1506	0.1552	
12	0.2129	0.1782	0.1430	0.1621	
13	0.2123	0.1683	0.1358	0.1530	
14	0.2110	0.1596	0.1294	0.1450	
15	0.2093	0.1518	0.1237	0.1379	

TABLE I: $\frac{E}{E}$ benchmark test cases for a charm jet ($m = 1.2$ GeV, $C_R = \frac{4}{3}$) with fixed $s = 0.3$. The path length is $L = 5$ fm; $hc = 0.197$ GeV fm. The density is $\frac{dN_g}{dy} = 1000$ ($n_f = 0$), giving $T = 0.2403$ GeV, $\epsilon = 0.4666$ GeV, and $\alpha_g = 1.2465$ fm. For radiative, the q integration limits are taken to be 0.0001 and 50.

C. Benchmark Numerical Examples

In this section we record numerical benchmark cases of both the elastic and radiative mean energy loss to illustrate the above formulas. Consider a uniform Bjorken cylinder with density

$$(\epsilon) = \frac{1}{R^2} \frac{dN}{dy} \quad (24)$$

We assume $R = 6$ fm. The temperature evolves as

$$T(\epsilon) = \frac{2}{1202} \frac{(\epsilon)}{9n_f + 16}^{\frac{1}{3}}$$

where n_f is the number of active quark flavors. The effective static approximation simulates the effect of Bjorken expansion by evaluating T at $\epsilon = L/2$, where L is the jet path length to the cylinder surface. The gluon density is computed from $\alpha_g = \frac{1.202}{2} 16T^3$, and the density of quarks plus antiquarks is $\alpha_q = \frac{1.202}{2} 9n_f T^3$. The Debye mass squared is $\epsilon^2 = 4 \frac{2T^2}{s} (1 + \frac{n_f}{6})$. In Table I the results for $n_f = 0$ are given for a charm jet of energy 10 GeV at 15 fm.

D. Energy Loss Fluctuation Spectrum

This section illustrates the fluctuation spectra of induced gluon number and the distribution of fluctuating energy loss for a specific case of a 15 GeV up quark jet with path length 5 fm. Fig. 9 shows the first order induced gluon number distribution dN_g/dx for this case. Fig. 10 shows the fractional radiative energy loss distribution taking into account Poisson fluctuations of the gluon number computed as in [4]. The finite probability, $P(n_g = 0) = 0.2377$, of radiating zero gluons contributes a peak that is not shown. There is also a finite probability, 0.0213, of complete stopping with $\epsilon > 1$.

The width of the elastic energy fluctuations seen in Fig. 11 is significantly smaller than the radiative width. The narrowing of the convoluted elastic plus radiative distributions significantly reduces the distortion effects

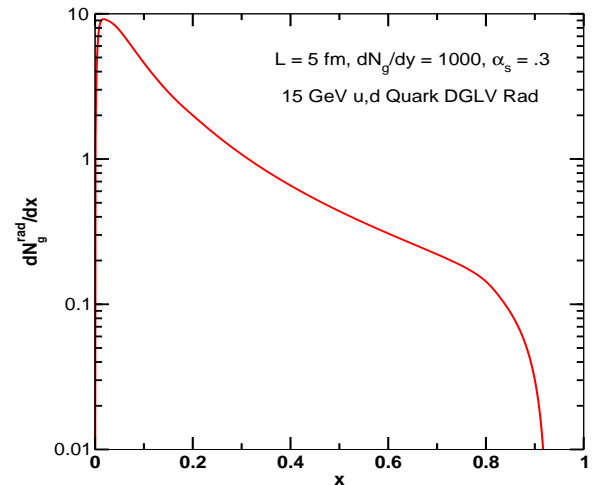


FIG. 9: Example of the induced DGLV radiation gluon number spectrum for a 15 GeV up quark, with path length $L = 5$ fm, $dN_g/dy = 1000$, $\alpha_s = 0.3$, and $A_2 = 118.7$ fm 2 .

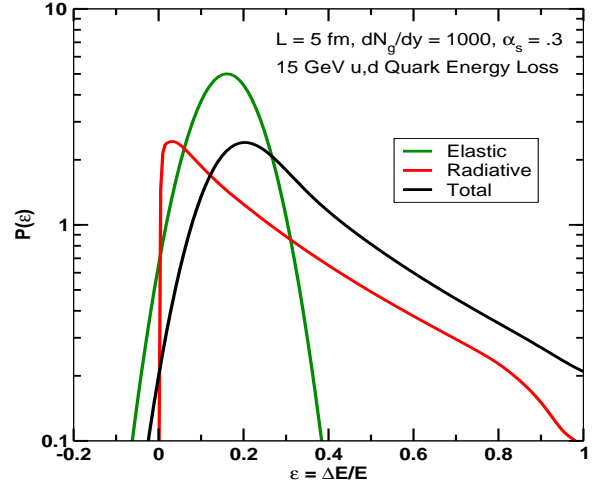


FIG. 10: The distribution of fractional radiative energy loss (or gain), $\epsilon = E/E$, for the case considered in Fig. 9. The narrow (green) curve corresponds to BT elastic energy loss fluctuations; based on the input from Fig. 9 the lower, broader (red) curve corresponds to inelastic energy loss due to gluon number fluctuations. The part of the radiation spectrum with $\epsilon > 1$ is replaced with 0.0213 (1 - x), and there is a contribution from zero gluon number fluctuations, 0.2377 (x), not shown. The continuous part of the radiative distribution has integrated norm 0.7374 with mean 0.2026. The top (black) curve corresponds to the convolution of elastic and inelastic energy fraction fluctuations.

due to fluctuations. Because of the steep p_T fall off of the initial unquenched parton spectra, the smaller width of the elastic energy fluctuations considerably amplifies the quenching effect due to collisional energy loss in comparison to the larger but much broader radiative contribution. In terms of an effective renormalization

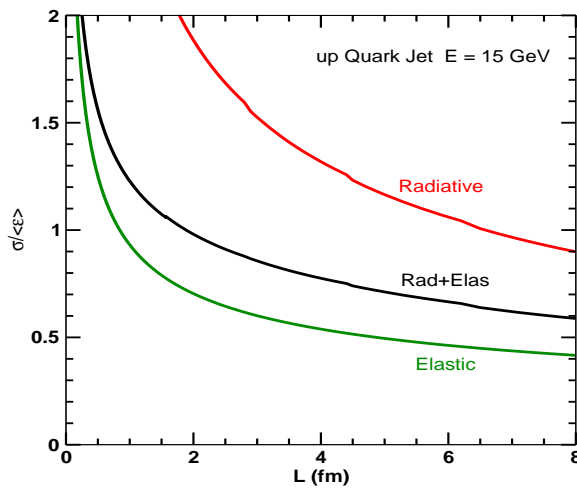


FIG. 11: The ratio of mean width, $\langle L \rangle$, to the mean fraction energy loss h is shown as a function of the path length, L , for the Bjorken expanding plasma with $dN_g/dy = 1000$. The case of an up quark jet with $E = 15$ GeV is shown. Notice that the elastic distribution is significantly narrower than the radiative one. This amplifies the effect of elastic energy loss on R_{AA} relative to radiative.

h is! $Z_{\text{eff}} h$ is as discussed in [4], Z_{eff} is closer to unity than the renormalization $Z_{\text{rad}} = 0.5$ characteristic of pure radiative energy loss distributions.

[1] T. Isobe, arXiv:nucl-ex/0510085. M. Shimomura [PHENIX Collaboration], arXiv:nucl-ex/0510023. S. S. Adler et al. [PHENIX Collaboration], Phys. Rev. Lett. 91, 072301 (2003) [arXiv:nucl-ex/0304022].

[2] M. G. Yulassy, I. Vitev, X. N. Wang and B. W. Zhang, Quark Gluon Plasma 3, (ed. R.C. Hwa and X.N. Wang, World Scientific, Singapore) pp. 123-191; nucl-th/0302077; A. Kovner and U. Wiedemann, pp. 192-248 op cit. [arXiv:hep-ph/0304151]; P. Jacobs and X. N. Wang, Prog. Part. Nucl. Phys. 54, 443 (2005) [arXiv:hep-ph/0405125]. X. N. Wang and M. G. Yulassy, Phys. Rev. Lett. 68, 1480 (1992).

[3] M. G. Yulassy, P. Levai and I. Vitev, Nucl. Phys. B 594, 371 (2001) [arXiv:nucl-th/0006010].

[4] M. G. Yulassy, P. Levai and I. Vitev, Phys. Lett. B 538, 282 (2002) [arXiv:nucl-th/0112071].

[5] I. Vitev and M. G. Yulassy, Phys. Rev. Lett. 89, 252301 (2002) [arXiv:hep-ph/0209161];

[6] S. S. Adler [PHENIX Collaboration], arXiv:nucl-ex/0510047; Y. Akiba [PHENIX Collaboration], arXiv:nucl-ex/0510008.

[7] J. Bialek [STAR Collab] arXiv:nucl-ex/0511005. X. Dong, [STAR Collab] arXiv:nucl-ex/0509038.

[8] M. D. Djordjevic, M. G. Yulassy, R. Vogt and S. Wicks, arXiv:nucl-th/0507019; Phys. Lett. B in press.

[9] New Discoveries at RHIC - the current case for the strongly interactive QGP", Proc. RBRC Workshop, May 14-15, 2004, BNL-72391-2004, Nucl. Phys. A 750, 1, 30, 64, 121 (2005).

[10] BRAHMS, PHOBOS, STAR, and PHENIX Collaborations, BNL-73847-2005; Nucl. Phys. A 757, 184 (2005), pp. 1, 28, 102, 184.

[11] BNL Press release, 4/18/05: http://www.bnl.gov/bnlweb/pubaf/pr/PR_display.asp?prID=05-38

[12] T. Hirano and M. G. Yulassy, [arXiv:nucl-th/0506049] and refs. therein.

[13] D. Winter (PHENIX), Quark Matter 2005 talk, <http://www.phenix.bnl.gov/phenix/WWW/publish/winter/QM2005/>

[14] R. Rapp, V. Greco and H. van Hees, arXiv:hep-ph/0510050.

[15] N. Armesto, A. Dainese, C. A. Salgado and U. A. Wiedemann, Phys. Rev. D 71, 054027 (2005) [arXiv:hep-ph/0501225].

[16] R. Baier, Nucl. Phys. A 715, 209 (2003) [arXiv:hep-ph/0209038].

[17] M. Cacciari, P. Nason and R. Vogt, arXiv:hep-ph/0502203.

[18] M. L. Mangano, P. Nason and G. Ridolfi, Nucl. Phys. B 373, 295 (1992).

[19] M. G. Mustafa, Phys. Rev. C 72, 014905 (2005) [arXiv:hep-ph/0412402]. M. G. Mustafa and M. H. Thoma, Acta Phys. Hung. A 22, 93 (2005) [arXiv:hep-ph/0311168].

[20] A. K. Dutt-Mazumder, J. e. Alam, P. Roy and B. Sinha, Phys. Rev. D 71, 094016 (2005) [arXiv:hep-ph/0411015].

[21] J. D. B. Bjorken, FERMILAB-PUB-82-059-THY (unpublished)

[22] M. H. Thoma and M. G. Yulassy, Nucl. Phys. B 351, 491 (1991).

[23] E. Braaten and M. H. Thoma, Phys. Rev. D 44, 1298 (1991). Phys. Rev. D 44, 2625 (1991).

[24] X. N. Wang, M. G. Yulassy and M. Plumier, Phys. Rev. D 51, 3436 (1995) [arXiv:hep-ph/9408344].

[25] M . G . M ustafa, D . Pal, D . K . Srivastava and M . Thom a, Phys. Lett. B 428, 234 (1998) [[arX iv:nucl-th/9711059](#)].

[26] Z . w . Lin, R . Vogt and X . N . W ang, Phys. Rev. C 57, 899 (1998) [[arX iv:nucl-th/9705006](#)].

[27] D . M olnar and M . Gyulassy, Nucl. Phys. A 697, 495 (2002) [Erratum -*ibid.* A 703, 893 (2002)] [[arX iv:nucl-th/0104073](#)].

[28] G . D . M oore and D . Teaney, Phys. Rev. C 71, 064904 (2005) [[arX iv:hep-ph/0412346](#)].

[29] Yu .L .D okshitzer and D .E .K harzeev Phys. Lett. B 519, 199 (2001) [[arX iv:hep-ph/0106202](#)].

[30] M . D . jordjević and M . G yulassy, Nucl. Phys. A 733, 265 (2004) [[arX iv:nucl-th/0310076](#)].

[31] M . D . jordjević and M . G yulassy, Phys. Rev. C 68, 034914 (2003) [[arX iv:nucl-th/0305062](#)].

[32] M . D . jordjević and M . G yulassy, Phys. Lett. B 560, 37 (2003) [[arX iv:nucl-th/0302069](#)].

[33] M . D . jordjević, M . G yulassy and S .W icks, Phys. Rev. Lett. 94, 112301 (2005) [[arX iv:hep-ph/0410372](#)].

[34] B .W .Zhang, E .W ang and X .N .W ang, Phys. Rev. Lett. 93, 072301 (2004) [[arX iv:nucl-th/0309040](#)].

[35] R . Vogt, Int. J. Mod. Phys. E 12, 211 (2003) [[arX iv:hep-ph/0111271](#)].

[36] J . Pumplin, D . R . Stump, J . Huston, H . L . Lai, P . Nadolsky and W . K . Tung, JHEP 0207, 012 (2002) [[arX iv:hep-ph/0201195](#)]; D . Stump, J . Huston, J . Pumplin, W . K . Tung, H . L . Lai, S .K uhlmann and J .F .O wens, [arX iv:hep-ph/0303013](#).

[37] I . V itev, Phys. Lett. B 562, 36 (2003) [[arX iv:nucl-th/0302002](#)]. ; J . Phys. G 31, S557 (2005) [[arX iv:hep-ph/0409297](#)]; J . W . Q iu, [arX iv:hep-ph/0507268](#).

[38] M .G yulassy, I .V itev and X .N .W ang, Phys. Rev. Lett. 86, 2537 (2001) [[arX iv:nucl-th/0012092](#)].

[39] K . J . Eskola, H . Honkanen, C . A . Salgado and U . A . W iedemann, Nucl. Phys. A 747, 511 (2005) [[arX iv:hep-ph/0406319](#)].

[40] B .H ahn, D .G .R avenhall and R .H ofstadter, Phys. Rev. 101, 1131 (1956).

[41] W .H orowitz, S .W icks, M .G yulassy, in preparation.

[42] S . Peigne, P . B . G ossiaux and T . G ousset, [arX iv:hep-ph/0509185](#).

[43] M .D .jordjević and M .G yulassy, Phys. Rev. C 68, 034914 (2003) [[arX iv:nucl-th/0305062](#)].

[44] A .Adil and M .G yulassy, in preparation.

[45] M .D .jordjević, [arX iv:nucl-th/0603066](#).

[46] X .N .W ang, [arX iv:nucl-th/0604040](#).

[47] M .D .jordjević, Phys. Rev. C 73, 044912 (2006) [arX iv:nucl-th/0512089](#).